Available online at www.sciencedirect.com

SciVerse ScienceDirect

Physics Procedia 37 (2012) 271 – 278

Physics Procedia

TIPP 2011 - Technology and Instrumentation in Particle Physics 2011

Status of the ATLAS Liquid Argon Calorimeter and its performance after one year of LHC operation

Julia Hoffman[1] - On behalf of the ATLAS Collaboration.

Southern Methodist University, Physics Department, 3215 Daniel Avenue, Dallas, TX 75205, USA

Abstract

The ATLAS experiment is designed to study the proton-proton collisions produced at the LHC with a centre-of-mass energy of 14 TeV. Liquid Argon (LAr) sampling calorimeters are used in ATLAS for all electromagnetic calorimetry covering the pseudorapidity region $|\eta|$ <3.2, as well as for hadronic calorimetry from $\eta = 1.4$ to $\eta = 4.8$. An overview of the system is shown as well as a discussion of its operation and performance at $\sqrt{s} = 900$ GeV and 7 TeV since the start of LHC running. The latest status of the detector as well as problems and solutions addressed during the last years are also discussed.

Keywords: ATLAS, Liquid Argon Calorimeter, LAr, LHC, LHC operation, CERN

1. Introduction

The ATLAS detector [1], shown in Figure 1, is one of the two general-purpose detectors at the LHC built for studying proton-proton collisions. Its structure is layered, consisting of three main systems of sub-detectors: the Inner Detector provides tracking up to a pseudorapidity[2]- $|\eta|$ - of 2.5, a calorimeter system with $|\eta|$ coverage up to 4.9 and a Muon Spectrometer, which provides $|\eta|$ coverage up to 2.7.

The ATLAS detector has been fully operational since 2008, starting with cosmic-ray data taking and commissioning. The acquisition of proton-proton (p-p) collision data began later, in November 2009, at $\sqrt{s} = 900$ GeV. After the end-of-the-year shutdown, the LHC resumed running in March 2010 with collision energies at $\sqrt{s} = 7$ TeV. The proton-proton collisions in 2010 were characterized by sufficiently low luminosity, where pile-up was not a major problem for detector performance studies. Since April 2011, luminosity delivery increased, leading up to about 10 p-p collisions per bunch crossing. The total luminosity recorded by ATLAS in 2010 and up until the conference in 2011 can be seen in Figures 2(a) and 2(b), respectively. Studies of the detector's performance under such conditions are in progress.

[1]Email: julia.hoffman@cern.ch

[2]In the ATLAS coordinate system, θ is the polar angle and ϕ is the azimuthal angle with respect to the beam axis. Pseudorapidity is defined as $\eta = -\ln\left[\tan\left(\frac{\theta}{2}\right)\right]$

1875-3892 © 2012 Published by Elsevier B.V. Selection and/or peer review under responsibility of the organizing committee for TIPP 11. Open access under CC BY-NC-ND license. doi:10.1016/j.phpro.2012.05.326

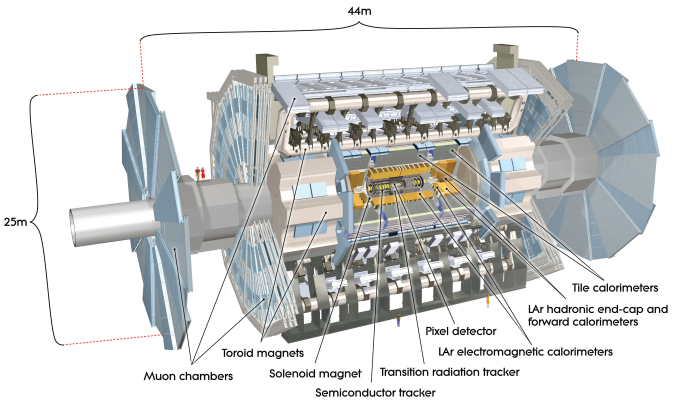

Fig. 1. The ATLAS Detector at the LHC.

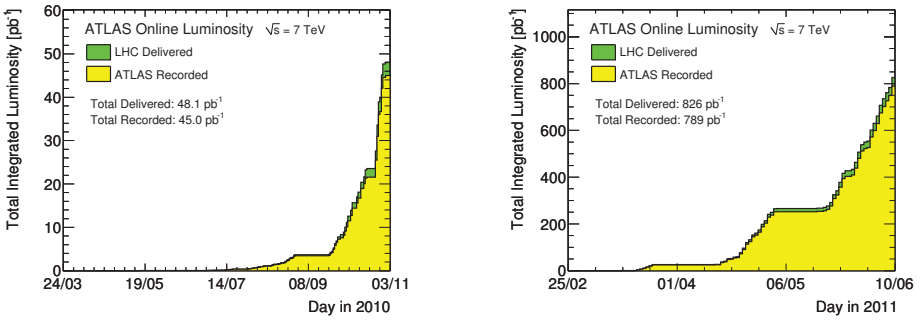

(a) Total luminosity recorded by ATLAS in 2010: 45.0 pb^{-1}.

(b) Total luminosity recorded by ATLAS by early June 2011: 789 pb^{-1}.

Fig. 2. Total integrated luminosity recorded by ATLAS in 2010 (a) and 2011 (b).

2. The ATLAS Liquid Argon Calorimeter

2.1. Design

For precise physics studies, high precision, high sensitivity, and high granularity calorimeters are needed in the ATLAS detector. The ATLAS Liquid Argon (LAr) calorimeter, illustrated in Figure 3(a), consists of an electromagnetic barrel (EMB) calorimeter - which incorporates a presampler (PS) - an electromagnetic endcap calorimeter (EMEC) , hadronic endcap calorimeter (HEC) and forward calorimeter (FCal).

The electromagnetic calorimeter uses liquid argon as an active medium and lead as the absorber. The accordion-shape geometry allows full azimuthal coverage with no cracks and coverage in $|\eta|$ up to 3.2. The choice of LAr as the active medium was based on the need for radiation hardness and for its fast and uniform response. The calorimeter is segmented in η, ϕ and depth. There are 3 layers in the EMB calorimeter after the presampler, c.f. Figure 3(b). The first layer is very finely segmented in order to provide excellent position resolution, which is necessary for good invariant mass resolution of electromagnetic final states, as well as $\gamma-\pi^0$ separation. A similar accordion-shape geometry was used for the EMEC. It consists of two concentric wheels: an outer wheel which provides coverage up to $|\eta| < 2.5$ with three longitudinal samplings and the inner wheel which provides two samplings out to $|\eta| < 3.2$. An endcap presampler provides coverage for $|\eta| < 1.8$. In the HEC, the absorber is copper. Each HEC is composed of two wheels with 32 wedge-shaped modules and has four layers arranged in a more conventional parallel-plate structure. Overall, the

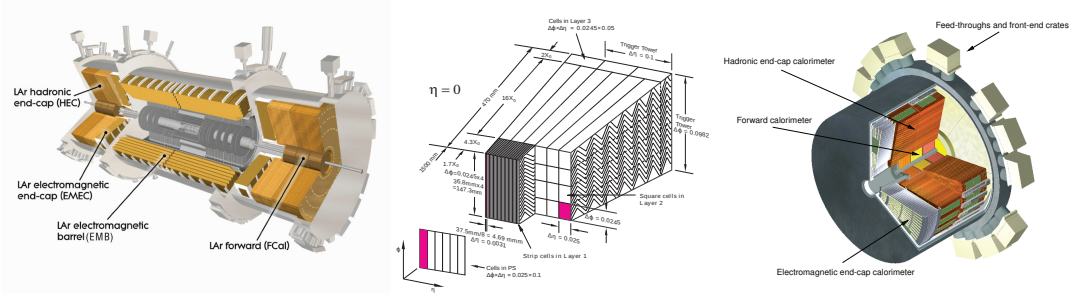

(a) (b) (c)

Fig. 3. The layout of the Liquid Argon Calorimeter (a). Accordion-structure and design of the electromagnetic barrel calorimeter (b). Overview of the endcap cryostat (c).

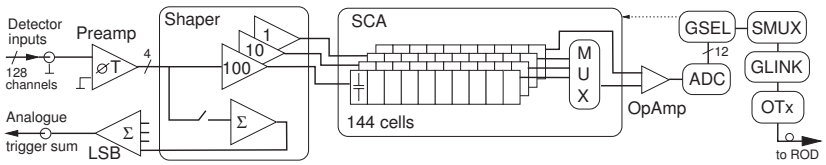

Fig. 4. Schematics of readout chain in the LAr FEB.

coverage provided by the HEC is $1.5 < |\eta| < 3.2$. The FCal, situated inside the HEC, provides coverage for $3.1 < |\eta| < 4.9$ and consists of three disk-shaped modules, with copper absorber for one electromagnetic layer and tungsten for two hadronic layers. Illustrations of the HEC and FCal are shown in Figure 3(c).

2.2. *Readout and Calibration*

Signals from the calorimeters are processed by front-end boards (FEBs) located in crates mounted directly on the cryogenic feedthroughs used to bring the signals out of the cryostat. Signals are amplified and shaped to provide a fast, bipolar signal. There are four outputs from the shaper, corresponding to three gains (each amplified by an order of magnitude) and an input to the analog sum for the trigger tower to which the channel belongs. There are 58 LAr front-end crates (FECs) with a total of 1,524 FEBs, each reading out up to 128 cells. The readout chain is illustrated in Figure 4.

The signal shapes are sampled every 25 nanoseconds; during normal operation this is synchronized with the LHC clock. Samples are stored in a Switched Capacitor Array analog pipeline until it reaches the Level-1 trigger (L1) signal, where they are read out and transmitted through optical fibers (one per FEB) to the back-end electronics outside the detector cavern. Readout Drivers (RODs) processes the samples using a digital filtering algorithm to calculate the signal amplitude (in MeV), timing, and a quality factor quantifying the agreement between the measured samples and the expected pulse shape. The digital-filtering procedure relies on calibration constants, which are monitored regularly and updated, when necessary, between ATLAS runs. The calibration scheme relies on good understanding of the pulse shape for each channel. Electronic calibration of the LAr system is performed through calibration boards installed in FECs. They provide calibration signals of known amplitude, with a shape that approximates that of the expected physics pulse. Three types of standard calibration runs are taken regularly to determine the required channel-by-channel calibration constants: Pedestal runs provide the ADC pedestal and noise values; Ramp runs determine the response to signals of increasing amplitude, for determination of the electronic gains; and Delay runs measure the response to calibration pulses with incremental timing offsets, for determination of pulse shapes. For a given calorimeter cell, the energy (E_{cell}) at the electromagnetic scale is computed as:

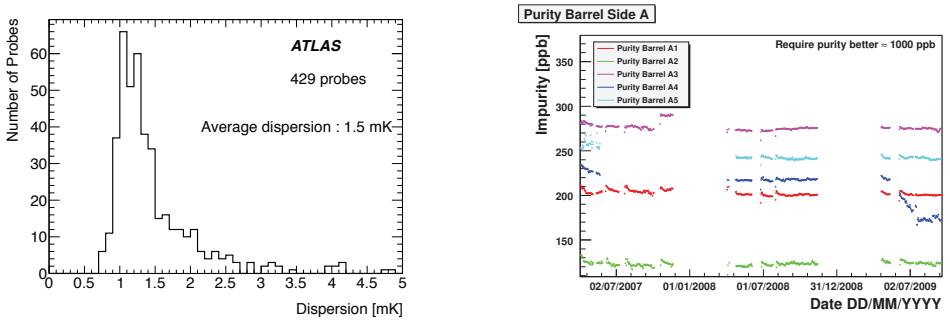

(a) (b)

Fig. 5. Temperature stability (a) and liquid argon purity (b) in the LAr Calorimeter.

$$E_{\text{cell}} = F_{\mu A\to\text{MeV}} \cdot F_{\text{DAC}\to\mu A} \cdot \frac{1}{\frac{M_{\text{phys}}}{M_{\text{cali}}}} \cdot R\left[\sum_{j=1}^{N_{samples}} a_j(s_j - p)\right],$$

where $F_{\mu A\to\text{MeV}}$ relates the ionization current in the detector to the deposited energy. $F_{\text{DAC}\to\mu A}$ describes the conversion between the digital-to-analog converter (DAC) setting on the calibration board and the amplitude of injected current pulse. The factor $\text{M}_{\text{phys}}/\text{M}_{\text{cali}}$ represents the ratio of the response between an ionization (physics) pulse and that of a calibration pulse with the same initial current. R is the gain of the channel obtained from the Ramp run described above, $(s_j - p)$ represents the pedestal-subtracted samples, in ADC counts, and a_j represents the optimal-filtering coefficients that are derived from the known pulse shape and noise for each channel. In normal running, the number of samples - $N_{samples}$ - is set to 5, but up to 32 samples can be taken; this is especially useful for pulse-shape studies. Calibrations are performed separately for each of the three gains used to cover the required dynamic range.

During the 2009 cosmic ray commissioning period, the calibration stability was monitored over a period of six months, over which time, the pedestal stability was better than 0.03 ADC counts and the gain stability was better than 0.1% [3]. An overview of the performance of the LAr readout electronics can be found in [4].

3. Detector Operation

The LAr calorimeters have been fully instrumented and operating at nominal high voltage since 2006; commissioning for the calorimeter started with cosmic ray interactions. ATLAS global cosmic ray running began in 2008 and was an important part of the commissioning of the detector and the Trigger and Data Acquisition (TDAQ) system. In September 2008, the first single beams were injected into the LHC. An accident on September 19, 2008 resulted with the shutdown of the LHC prior to its first collisions. Beams were reintroduced into the LHC in November 2009 with first collisions starting at $\sqrt{s}$ = 900 GeV. Since March 2010, the LHC has been running at an energy of 3.5 TeV per beam. Running at this energy is planned to continue through to the end of 2012.

The performance of the detector has been very good throughout the commissioning and early data-taking phases. An example of excellent performance is the temperature and purity of liquid argon. The temperature homogeneity of LAr within each cryostat has averaged 59 mK with a dispersion of 1.5 mK where the design requirement is no more than 100 mK. The purity of LAr is important for signal collection, it is also well within the required limits in each cryostat. The impurity level is 200 ± 100 ppb (O_2 equivalent), when it is required to be less than 1000 ppb. Temperature stability and liquid argon purity is shown in Figure 5(a) and 5(b).

As the detector has continued running, the LAr calorimeter has experienced problems with Optical Transmitter Links, Low Voltage Power Supplies (LVPS) and High Voltage (HV) Power Supply trips; none of which affected the quality of running.

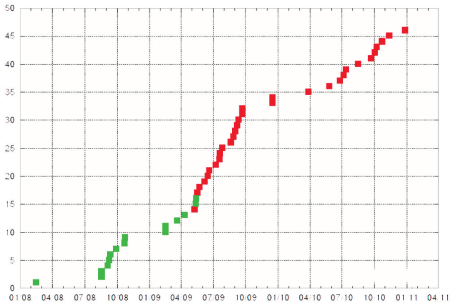

(a) Green squares represent the FEBs replaced during the shutdown in 2009. Red squares represent the failures since the shutdown.

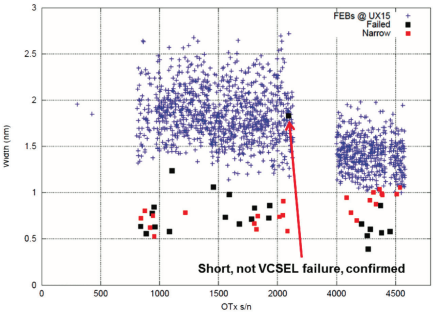

(b) Blue pluses represent the width of each FEB, black squares represent those FEBs which failed and red squares represent FEBs with narrow widths.

Fig. 6. Cumulative Optical Transmitter failures since January 2008 (a) and the optical spectrum width of the VCSEL (b).

3.1. Hardware Problems

An optical transmitters (OTx), one per FEB, is used to transmit the data to the back-end system. An OTx failure means that no data is transmitted for the entire FEB. Optical transmitters are on-detector electronics where access is not possible except during extended shutdown periods. OTx failure became an issue in 2008, where there was about 1 failure per week. Figure 6(a) shows the cumulative number of OTx failures as a function of time, since 2008. During the 2008-2009 shutdown, failed electronics were replaced, but new ones were as reported failing. The cause of this problem was extensively investigated. While no definitive explanation was found, investigations of the on-detector OTx showed that almost all OTx failures were confirmed or consistent with Vertical Cavity Surface Emitting Lasers (VCSEL) failures. The failure of the VCSEL is not completely understood, but a possible explanation is that there was an electrostatic discharge. During such an event, the optical spectrum changes, measured as being narrower than expected. The discharge defect grows with time until the unit fails. The optical spectrum width of the VCSEL is a good indicator for potential damage (Figure 6(b)). After an OTx exchange during the winter 2010-2011 shutdown, no failures were reported. Despite many OTx failures, it was not fatal to the experiment; data analyses excluded the affected regions.

The Low Voltage Power supplies also had problems. The LVPS contain DC-DC converters that provide the various voltages that are required by the Front-End electronics. The LVPS were a source of early problems during long-term burn-in tests and after installation on the detector. There have been no full failures since the start of LHC collisions, only losses in LVPS redundancy. The uncertainty of their reliability has lead to the design and manufacturing of new supplies.

The High Voltage Power Supplies provide drift voltage across the LAr gaps in the calorimeters between electrodes and absorbers. Each electrode is powered from the back by two separate HV lines. Roughly 6% of the channels need HV corrections due to occurring trips. The value of the correction factor depends on affected channel and varies from 1 to 2. HV trips are correlated with the presence of collisions. In a sequence of steady fills with the same luminosity and number of bunches, the number of trips decreases with each fill.

In spite of these problems, the LAr EM calorimeter (EMB and EMEC) operates at an efficiency of 99.8%, whereas the HEC and FCal respectively operate at 99.6% and 99.8%.

3.2. LAr Timing Studies

A good understanding of LAr timing measurements is useful for distinguishing between energy deposits resulting from triggered beam crossing and those from neighbouring bunch crossings. These measurements are useful in helping veto cosmic ray events against collisions events. Longitudinal segmentation and timing can also be used to identify non-pointing photons. FEB time offsets in nanoseconds for the 4 partitions of

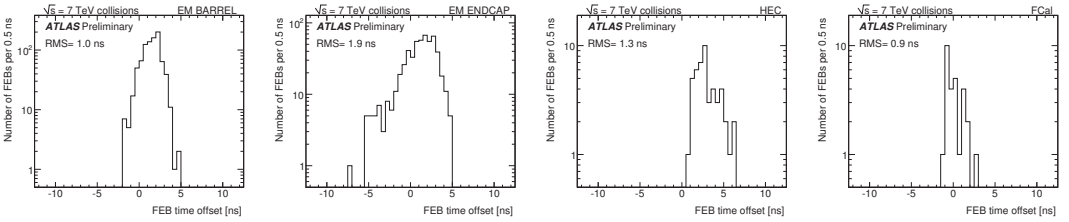

Fig. 7. FEB time offsets (in ns) for the barrel (a), endcap (b), hadronic endcap (c), and forward calorimeter (d).

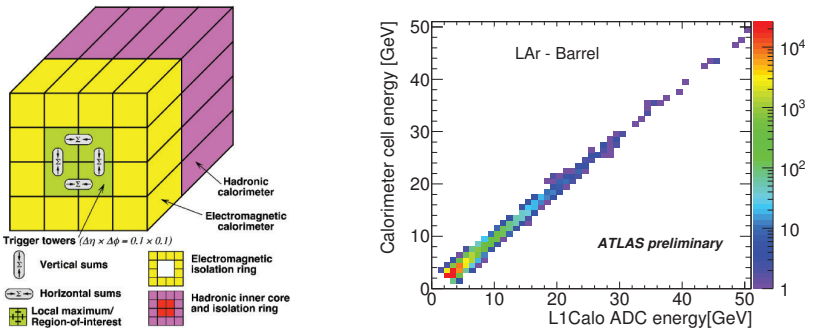

Fig. 8. Level 1 trigger schema (a). Scatter plot of transverse energy measured by the calorimeter vs. the Level 1 trigger (b).

the detector - barrel, endcap, hadronic endap, and forward calorimeter are shown in Figures 7(a), 7(b), 7(c), and 7(d), respectively. Coarse time adjustments are done with configurable delays of each FEB. Finer adjustments can be made per channel by using optimal filtering coefficients. The goal is a timing resolution of approximately 100 ps.

3.3. Trigger Performance

The calorimeter trigger schema is presented in Figure 8(a). The schema shows how trigger towers, each in $\eta \times \phi$ region of 0.1 ×0.1 (about 60 readout channels), are used to determine the energy of the electromagnetic cluster as well as for electromagnetic isolation, hadronic core and hadronic isolation. Figure 8(b) shows the energy correlation from 7 TeV data where the transverse energy measured in the LAr Calorimeter is shown vs. the transverse energy measured by Level 1 trigger. The transverse energy of all cells which correspond to a Trigger Tower is summed up and compared to the corresponding L1 Trigger Tower. The correlation is good, where the resolution of the transverse energy in the L1Calo is less than 5% for transverse energies greater than 10 GeV in the LAr calorimeter.

4. Performance Studies With Data

One of the primary functions of the ATLAS detector is to measure the energy of jets, electrons, photons, transverse energy, and missing transverse energy of events. It is important that discrepancies between data and Monte Carlo are studied and understood. These discrepancies can be caused by new and unmodeled physics or inadequacies in detector simulation. Numerous studies have been performed using collision data. These studies helped refine the EM energy scale (via Z→ee and J/Ψ →ee production), performance of missing energy, and even refine $\gamma - \pi^0$ separation.

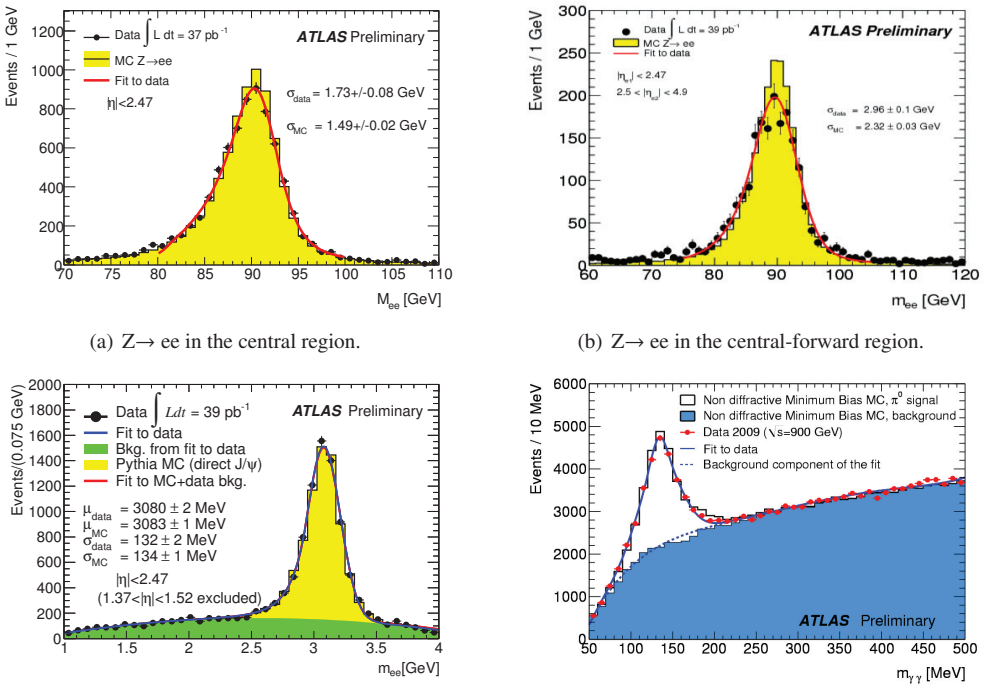

(a) Z→ ee in the central region.

(b) Z→ ee in the central-forward region.

(c) J/Ψ → ee.

(d) $\pi^0 \rightarrow \gamma\gamma$.

Fig. 9. Invariant mass distribution of Z→ ee in the central region (a) central-forward region (b) of ATLAS. Invariant mass distribution of J/Ψ (c) and π^0 (d).

4.1. EM Energy Scale Uniformity

The scale and uniformity of energy is checked over the full acceptance of the LAr calorimeter by using data to reconstruct well-known resonances decaying to electromagnetic final states. The response to high-p_T ($p_T > 20$ GeV) electrons has been studied using Z→ee decays and corrections to the energy scale were made (Figure 9(a)). Using the re-calibrated energy scale, the Z→ee decays were also used to study the EM scale in the forward region, for $|\eta| > 2.5$, where, due to the absence of tracking, electrons are identified based on cluster shapes in the calorimeter (Figure 9(b)). Lower p_T electrons were studied by looking at di-electron decays of J/Ψ (Figure 9(c)). The results of the analysis yielded excellent agreement. A similar study was performed using photons in pion decays in 900 GeV collision data [5], the agreement is between data and Monte Carlo is good, as seen in Figure 9(d), it pre-dates the corrections made by the Z→ee and J/Ψ →ee analyses.

4.2. Missing Transverse Energy

Missing transverse energy is a characteristic signature for the production of massive particles that escape detection as predicted in many theories beyond the Standard Model. Figure 10(a) shows a distribution of missing transverse energy as measured in a 2010 data sample of minimum bias events at 7 TeV, further explained in [6]. Energies are calibrated using Local Cluster Weighting (LCW). There is good agreement between data and Monte Carlo. Figure 10(b) shows the distribution of transverse energy for electrons passing certain selection criteria, there is very good agreement between data and Monte Carlo.

5. Summary

The ATLAS LAr calorimeter is designed to accurately measure the transverse energy of electrons, photons, jets, and missing transverse energy of events with good precision. Instrumentation was completed

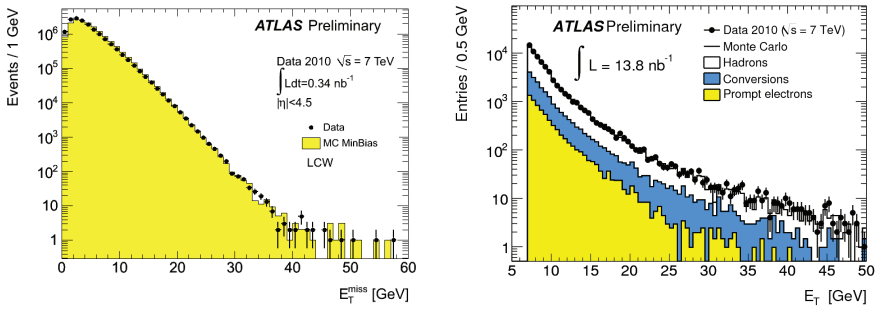

(a) (b)

Fig. 10. Distributions of missing transverse energy (a) and transverse energy (b) in data and Monte Carlo.

in 2006 and it has been operating at nominal voltage since then. The most serious problems encountered throughout commissioning and data-taking include the failures of optical transmitters, loss of redundancy in low voltage power supplies, and high voltage trips. Most of these problems have either been resolved or worked on, with some studies still in progress; overall the quality of detector operation is not affected. The LAr calorimeter is well understood despite these problems and its performance has been excellent, near design expectations.

References

[1] The ATLAS Experiment at the CERN Large Hadron Collider, G. Aad et al., JINST **3** (2008) S08003.
[2] LHC machine, L. Evans and P. Bryant eds., JINST **3** (2008) S08001.
[3] Readiness of the ATLAS Liquid Argon Calorimeter for LHC Collisions, G. Aad et al., Eur. Phys. J. C 70 (2010) 723.
[4] Performance of the electronic readout of the ATLAS liquid argon calorimeters, H. Abreu et al, JINST 5 (2010) P09003.
[5] Performance of the ATLAS electromagnetic calorimeter for $\pi^0 \to \gamma\gamma$ and $\eta \to \gamma\gamma$ events., ATLAS Collaboration, ATLAS-CONF-2010-006 (2010).
[6] Performance of the Missing Transverse Energy Reconstruction and Calibration in Proton-Proton Collisions at a Center-of-Mass Energy of $\sqrt{s} = 7$ TeV with the ATLAS Detector. ATLAS Collaboration, ATLAS-CONF-2010-057, (2010).